ACADEMIC PRESS

Available online at www.sciencedirect.com

SCIENCE DIRECT®

Journal of Sound and Vibration 263 (2003) 515–533

JOURNAL OF SOUND AND VIBRATION

www.elsevier.com/locate/jsvi

Moment excitation of structures using two synchronized impact hammers

Y. Champoux, V. Cotoni*, B. Paillard, O. Beslin

Groupe d'Acoustique et Vibrations de l'Université de Sherbrooke (GAUS), Sherbrooke, Qué., Canada J1K 2R1

Received 28 January 2002; accepted 25 June 2002

Abstract

Moment mobilities are difficult to measure because there is no simple way to excite a structure with a well-controlled moment. In this paper, a technique to apply a nearly pure moment is presented. It is based on a simple approach that uses two impact forces applied, respectively, by two impact hammers. The limits and the validity of this approach are first examined theoretically on a simply supported plate. Comparisons between the excitation by two distant opposite forces and by a pure moment are performed. Then, the coupling between the two hammers and the structure during the impact phase is considered in order to analyze practical limits of obtaining identical forces impacting at different locations. Finally, a detailed description of the experimental system developed to obtain identical synchronized forces is presented. Two hammers driven by electric motors controlled by a Digital Signal Processor are used. Experimental results are compared to theoretical predictions. It is shown that the technique yields accurate measurements of moment frequency response functions.

1. Introduction

For a complete characterization of a dynamic system, moment mobility measurements are required since all six degrees of freedom are of interest [1,2]. Exciting a structure with only a moment component poses numerous difficulties. Several methods have been proposed in the past [3–5]. Attaching two shakers directly to the structure or through an attachment fixture is the traditional method. A global approach requires to attach a six-degree-of-freedom transducer [6]. Some techniques use an intermediate T-like structure or an I-like beam [7,8] to impose simultaneously moments and forces. None of these techniques succeeds in easily applying only a moment component, and some of them require complex post-analysis to extract the different excitation components.

*Corresponding author.
E-mail address: vincent.cotoni@gaus.gme.usherb.ca (V. Cotoni).

0022-460X/03/$ - see front matter
PII: S0022-460X(02)01064-7

In this paper, a technique is proposed to excite a structure with a nearly pure moment obtained from a force couple. Part of this study has been presented in Refs. [9,10]. The technique is based on a simple approach that uses two impact forces applied by two hammers as detailed in Section 2. These two, ideally identical forces have parallel lines of action, separated by a known distance, and are opposite in direction. In the simplest configuration the forces are applied on both sides of the structure. If only one side is available, an additional I-beam or T-beam can be used to transmit the couple. The time varying moment is the product of the instantaneous force amplitude multiplied by the distance between them. The strengths and weaknesses of this moment excitation technique by impact are the same as those of the force impact technique [11,12]. The main advantage of this approach compared to previous ones is that it allows the excitation of the structure with only a moment of a couple. Furthermore, the quality of the applied excitation can be monitored and evaluated during the test since no post-analysis needs to be achieved.

The implementation of this apparently simple approach poses, however, some difficulties. Rigorously, two forces separated by a small distance cannot generate a high amplitude localized moment. The distance between the lines of action of the forces must not be too small, unless the applied forces have a very high amplitude. This aspect is studied in Section 3 by comparing the mobilities generated by two identical forces and by a pure moment. Also, the two impact hammers are sensitive to the local input impedance of the structure, which can be different for the two application points. When this is the case, it affects differently the time varying shape of each force, which does not allow one to excite the structure with a pure couple. To study the limits and the validity of the approach, a theoretical model has been developed and is presented in Section 4. The model takes into account the coupling between the impact hammers and the structure. Each impact hammer is modelled by a one-degree-of-freedom system. The characteristics of the hammer are identified from experimental measurements. The influence of several parameters is examined through the comparison of the predicted mobilities obtained with two strictly identical forces or with two realistic forces.

The experimental implementation of the technique is described in Section 5. Two miniature impact hammers driven by two brushless electric motors controlled by a Digital Signal Processor are used. It is shown that automatic calibration and adjustment techniques based on an energy comparison scheme allow one to obtain two nearly identical forces. It is possible to have a direct estimation of the quality of the measurement if, for example, one measures simultaneously the frequency response functions (FRFs) between a given output and the two input forces. Indeed, the two FRFs are identical only if the forces are identical. Comparisons between theoretical and experimental moment accelerance FRFs are presented. It is shown that the technique is viable and can give reliable results. Due to the application of two distinct forces to generate a couple, the force separation distance and the force amplitude have to be selected to cover the desired frequency range.

2. Basics of the technique

The technique can be used in the different configurations shown in Fig. 1. The two forces F_1 and F_2 are always parallel and opposite in direction. The forces separated by a distance d generate a moment M_C, which is considered to be applied at mid-distance between the application points of

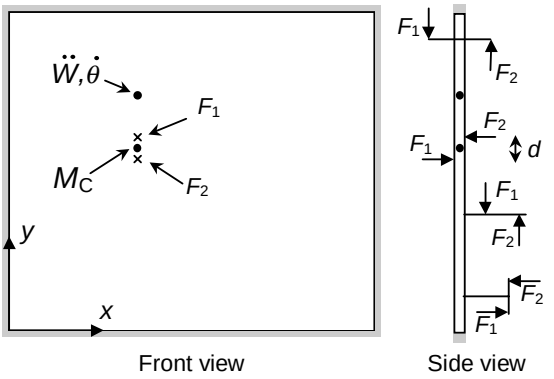

Fig. 1. Plate showing the points of application of the forces and of the response. Several configurations of excitation are shown on the side view.

the two forces. Assuming that both forces are identical, the moment amplitude is simply $M_C = Fd$. When possible, the forces are applied on both sides of the structure. A small I- or T-beam can also be used to transmit the excitation. In these latest cases, corrections must be performed to take into account the loading effects of the moment exciter devices [2]. Nevertheless, the advantage of generating an almost pure moment remains.

In this paper, the configuration with forces on both sides of the structure is used for sake of simplicity and to avoid a post-analysis. The limit of validity of generating a moment using two identical forces is first examined.

3. Moment using two forces

Two forces separated by a distance of few centimeters cannot apply a theoretical point moment to a structure. The situation is equivalent to the measurement of acoustic intensity using two microphones. The main systematic error is inherent in the approximation of the force gradient by a finite force difference. However in practice, as it will be shown, this approach frequently yields accurate results but imposes a high-frequency limitation.

To examine the importance of this limitation, the rotational moment mobility generated by a localized moment is compared to the moment mobility generated by two forces. A Love–Kirchhoff simply supported plate (sine mode shapes) is used for the calculation. For the same frequency span, two plate thicknesses and two plate separation distances are selected. Results are shown in Figs. 2 and 3. The curves peak differences are provided with the arrows and the value in dB near each peak.

For a thin plate and for a distance d of 3 cm (Fig. 2a), a moment generated by two forces gives an accurate estimation of the moment mobility. As d is increased to 10 cm, some discrepancies appear in the higher frequencies (Fig. 2b). For a thicker plate as shown in Fig. 3, even a large value of d gives acceptable results for almost all the modes in the shown frequency span. As indicated in Ref. [13], the structural wavelength of the mode relative to the distance d is the dominant factor. For both thicknesses, the error on the magnitude of the resonance peaks remains

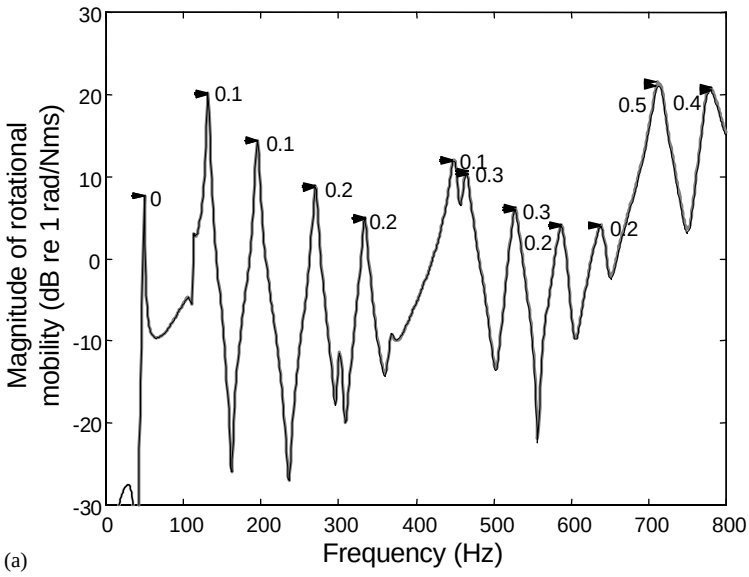

(a)

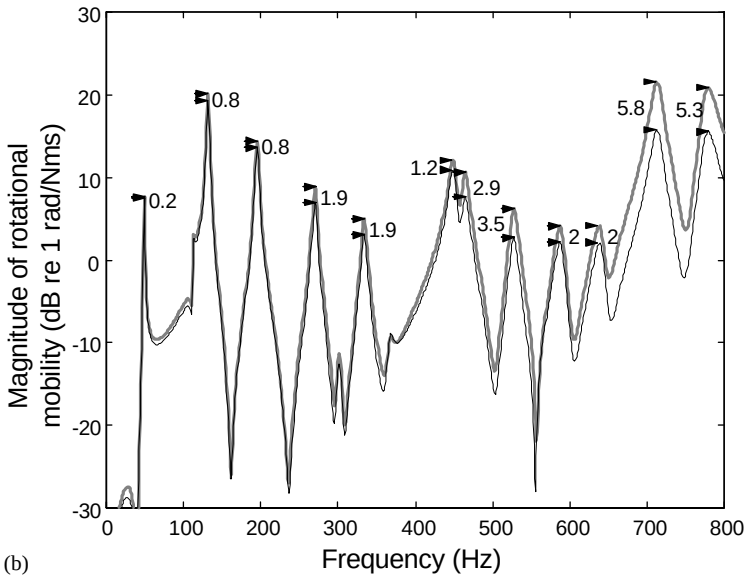

(b)

Fig. 2. Comparison between the localized rotational moment mobility (——) and the rotational mobility generated by two forces (——) for two distances d between the forces. Plate thickness: $h = 2$ mm. (a) $d = 3$ cm; (b) $d = 10$ cm.

smaller than 2 dB for modes with the wavelength in the direction of d larger than $2d$. For a distance d of 10 cm, this high-frequency limit corresponds to the mode at 366 Hz for the thin plate (Fig. 2b) and 583 Hz for the thick plate (Fig. 3). This analysis is quantitatively confined to the case of thin plates but is qualitatively general and consistent with the observation made in Ref. [13] concerning the measurement of rotation by the finite difference approximation.

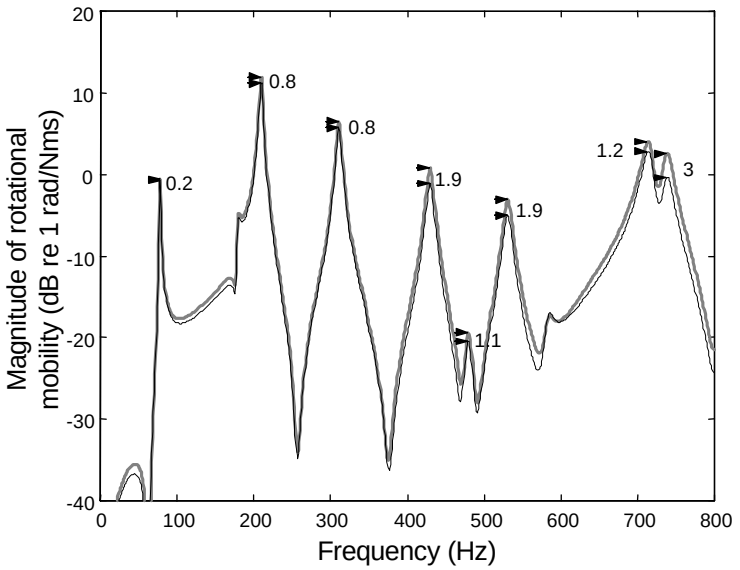

Fig. 3. Comparison between the localized rotational moment mobility (——) and the rotational mobility generated by two forces (——) for a plate of thickness $h = 3.18$ mm and a distance between the forces of $d = 10$ cm.

4. Theoretical model of impact

The objective of this section is to examine the feasibility of using two impact hammers to generate two simultaneous identical forces. Since the hammer hits at two separate locations on the structure, the local stiffnesses as seen, respectively, by each hammer are necessarily different. It is thus important to check if the coupling between the hammer's response and the structure influences the forces noticeably and differently. It is worth to remember that if one wants to apply a nearly pure moment, the forces have to be nearly identical.

4.1. Hammer model

The objective is to obtain a simple tool to analyze the coupling between the structure and the hammer. For sake of simplicity, a simple one-degree-of-freedom model is used to predict the vibration behavior of the hammer as shown in Fig. 4. The soft tip is represented by a spring with a stiffness constant k_1 and a viscous dashpot with a damping coefficient c_1. The hammer tip, the force transducer and the hammer head masses are represented by the mass m_1. The displacement of the mass is x_1.

A PCB general-purpose impact hammer equipped with a soft-plastic tip (nylon) is used to impact a nearly rigid wall with a very low point mobility. The appropriate values for k_1, c_1, and m_1 are determined through curve fitting on the impact force time history. The applied force is $F = k_1 x_1 + c_1 \dot{x}_1$, and the initial conditions at $t = 0$ s are $x_1(0) = 0$ and $\dot{x}_1(0) = v_0$, where v_0 is the known impact velocity. Since the force is null at the beginning of the impact, $F(0) = c_1 v_0 \approx 0$, the curve fitting leads to a small value for the damping parameter c_1. Fig. 5 compares the measured impact force time history with the prediction of the identified model. The discrepancy is relatively

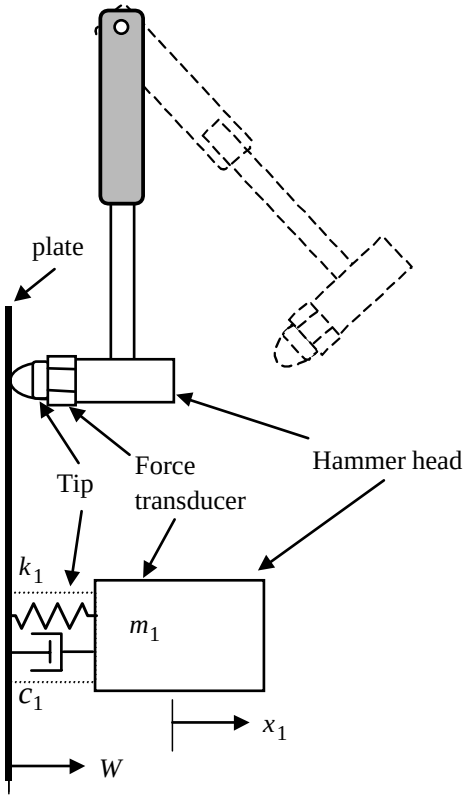

Fig. 4. Impact hammer model.

small keeping in mind that the objective of using a one-degree-of-freedom model is to have simple means to represent the behavior of the hammer. To have a more accurate model, one would need to take into account that the stiffness k_1 is not constant because the round part of the tip changes shape during the impact, especially for strong impacts.

4.2. Plate–hammer model

4.2.1. Time domain model of a hammer impact

In this section, a model that couples the previously developed hammer model with a simply supported plate is presented. During the impact phase, the system is represented as a coupled plate–spring–mass system (damping is neglected since it was shown to be typically very small). The mode shapes during the contact phase are consequently not sinusoidal. At the end of the impact, the hammer looses contact with the plate, and the plate vibrates freely according to its natural sine modes.

The Love–Kirchhoff model for the normal displacement $W(P,t)$ of the plate is used

$$D\nabla^4 W(P,t) + \rho h \frac{\partial^2 W(P,t)}{\partial t^2} = F_1(t)\delta(P,P_1), \tag{1}$$

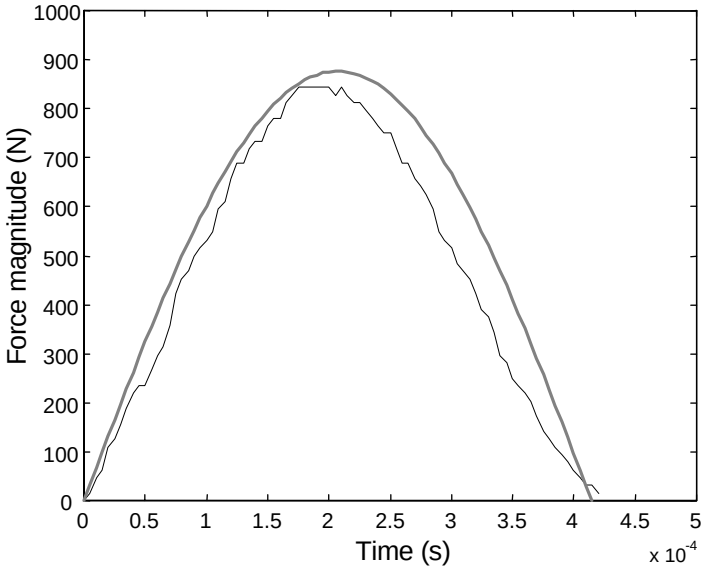

Fig. 5. Experimental and identified time history of the force applied by an impact hammer. Identified parameters: $m_1 = 0.087\,\text{kg}$, $k_1 = 5 \times 10^6\,\text{N/m}$, $c_1 = 0\,\text{N s/m}$; ——, experimental result; ▬, model.

$$D = \frac{Eh^3}{12(1-\nu^2)}, \tag{2}$$

where D is the plate bending stiffness, E the Young's modulus, h the plate thickness, ν the Poisson ratio, ρ the mass per unit area, P the location of the current point, P_1 the location of the impact point, t the time, $F_1(t)$ the force between the plate and the hammer, and $\delta(P, P_1)$ the Dirac distribution.

The plate displacement is sought as an expansion in the natural modes $\{\varphi_{mn}\}$ of the simply supported plate

$$W(P,t) = \sum_m \sum_n w_{mn}(t)\varphi_{mn}(P), \tag{3}$$

with

$$\varphi_{mn}(P) = \sin\left(\frac{m\pi x}{a}\right)\sin\left(\frac{n\pi y}{b}\right), \tag{4}$$

where a and b represent, respectively, the length and height of the plate. The definition of coordinates x and y are shown in Fig. 1. The equation of motion of the hammer is

$$m_1\ddot{x}_1(t) + k_1(x_1(t) - W(P_1,t)) = 0, \tag{5}$$

where x_1 denotes the displacement of the force transducer as shown in Fig. 4, and $\dot{}$ the differentiation with respect to time. The force of the hammer $F_1(t)$ acting on the plate is given by

$$F_1(t) = k_1(x_1(t) - W(P_1,t)). \tag{6}$$

When the hammer loses contact with the plate, the hammer force F_1 is set to zero. Projecting Eq. (1) on the basis functions $\{\varphi_{mn}\}$ and substituting Eqs. (5) and (6), the following linear system is obtained:

$$\mathbf{M}\ddot{\mathbf{X}}(t) + \mathbf{K}\mathbf{X}(t) = 0, \tag{7}$$

where

$$\mathbf{X}(t) = \begin{bmatrix} w_{11}(t) \\ \vdots \\ w_{mn}(t) \\ \vdots \\ x_1(t) \end{bmatrix}. \tag{8}$$

The generalized mass $\mathbf{M}$ and stiffness $\mathbf{K}$ matrices are given in Eqs. (9) and (10), where the value of the function $\varphi_{mn}(P)$ evaluated at the point P_1 is denoted φ_{mn}:

$$\mathbf{M} = \rho\frac{ab}{4}\begin{bmatrix} 1 & 0 & \cdots & 0 \\ & 1 & & \vdots \\ & & \ddots & 0 \\ sym & & & \dfrac{4m_1}{\rho ab} \end{bmatrix}, \tag{9}$$

$$\mathbf{K} = \begin{bmatrix} K_{11} + k_1\varphi_{11}\varphi_{11} & \cdots & k_1\varphi_{11}\varphi_{mn} & \cdots & -k_1\varphi_{11} \\ & \ddots & & & \vdots \\ & & K_{mn} + k_1\varphi_{mn}\varphi_{mn} & & -k_1\varphi_{mn} \\ & & & \ddots & \vdots \\ sym & & & & -k_1 \end{bmatrix} \tag{10}$$

with

$$K_{mn} = \frac{ab}{4}D\left\{\left(\frac{m\pi}{a}\right)^2 + \left(\frac{n\pi}{b}\right)^2\right\}. \tag{11}$$

The modes of the plate–hammer system are calculated by solving the generalized eigenvalue problem

$$\mathbf{P}^{\mathrm{T}}\mathbf{M}\mathbf{P} = [\delta_{ij}], \quad \mathbf{P}^{\mathrm{T}}\mathbf{K}\mathbf{P} = [\omega_i^2\delta_{ij}], \tag{12}$$

where $\mathbf{P}$ is the mass normalized transfer matrix from the coupled system's modal basis to the plate's modal basis, and ω_i are the natural frequencies. Using the matrix $\mathbf{P}$, the following system of uncoupled equations is obtained:

$$\ddot{\mathbf{R}}(t) + \tilde{\mathbf{K}}\mathbf{R}(t) = 0, \tag{13}$$

where $\tilde{\mathbf{K}}$ is a diagonal stiffness matrix and $\mathbf{R}$ is the vector of modal coordinates given by

$$\mathbf{X}(t) = \mathbf{P}\mathbf{R}(t). \tag{14}$$

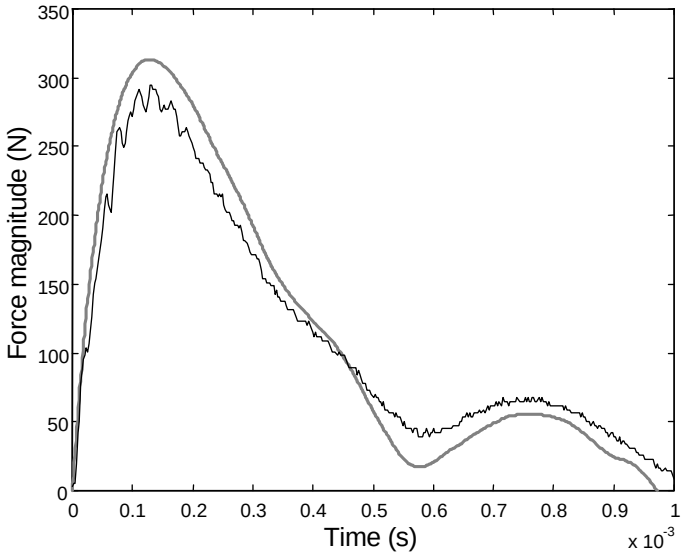

Fig. 6. Comparison of the experimental and calculated force time histories. Plate dimensions: $a = 48$ cm, $b = 42$ cm, $h = 3.18$ mm; impact point coordinates (15 cm, 15 cm); ——, experimental result; ▬, model.

For an impact test, initial conditions at time $t = 0$ s are $W(P,0) = \dot{W}(P,0) = 0$, $x_1(0) = 0$ and $\dot{x}_1(0) = v_0$, where v_0 is the known impact velocity. Expressing these initial conditions in modal coordinates, the solution of Eq. (13) can be calculated. The solution $\mathbf{X}(t)$ is then determined with Eq. (14).

4.2.2. *Experimental validation of the force hammer–plate mode*

The model involving one hammer is validated experimentally using a simply supported 42 cm × 48 cm × 3.18 mm aluminum plate. The hammer characteristics were identified with a test on a nearly rigid wall, as shown in Section 4.1. A comparison between the predicted force and the measured force during an impact on the elastic plate is shown in Fig. 6. The results are excellent given the very simple model used to represent the behavior of the impact hammer. The force has no longer the half sine shape shown in Fig. 5 for an impact on a rigid wall because the coupling between the hammer and the plate influences the impact force.

The model can be easily expanded to a double hammer impact by introducing a second hammer with characteristics k_2, m_2. An equation equivalent to Eq. (6) is used to estimate the force applied to the plate by the second hammer at an impact point P_2. The size of the matrices is augmented in order to take into account the extra degree of freedom x_2.

4.3. *Comparison analysis of two synchronized impact forces*

A suitable two hammers–plate model being available, the possibility of generating two identical impact forces is examined in this section. The influence of the distance d on the time variations of the two applied forces is analyzed. All the results are given for the case where the two hammers apply a force directly on each side of the plate. In Fig. 7, three plate thicknesses are considered.

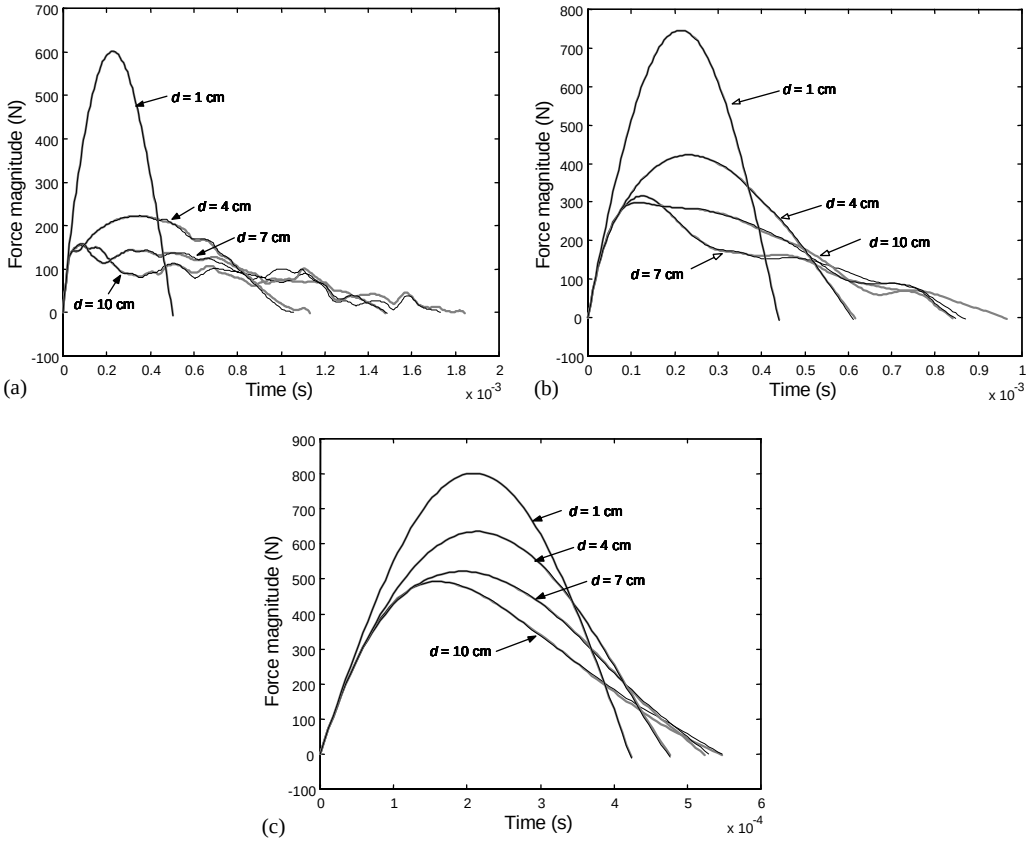

Fig. 7. Comparison of the time variations of forces F_1 and F_2 for different force separation distances d for three plate thicknesses. (a) $h = 2$ mm; (b) $h = 3.18$ mm; (c) $h = 5$ mm. ▬, force 1; ——, force 2.

The time variations of both forces are presented for several values of d. For a thin plate and a large value of d, the coupling between the plate and the hammer influences differently the two forces, meaning that the input impedances are different, with the consequence that the time histories are distinct. For a thicker plate or smaller values of d, both forces are indistinguishable, and a couple is obtained. Increasing the distance d or reducing the plate thickness have in fact the same effect on the relative length of the separating distance and the wavelength of the modes of the plate. As noted before, this is the main factor controlling the behavior of the two impact forces.

A similar analysis can be done in the frequency domain. The force spectra of F_1 and F_2 for three values of d are shown in Fig. 8. The 6 curves correspond to the curves shown in Fig. 7b ($h = 3.18$ mm) for the specified values of d. For an impact technique, it is common practice to fix a high-frequency limit for the test, which corresponds to a 10 dB drop in the force energy magnitude. For this usable frequency range, Fig. 8 shows that the two force spectra are indistinguishable. In practice, the two force spectra can be measured to check the accuracy of the pure couple assumption.

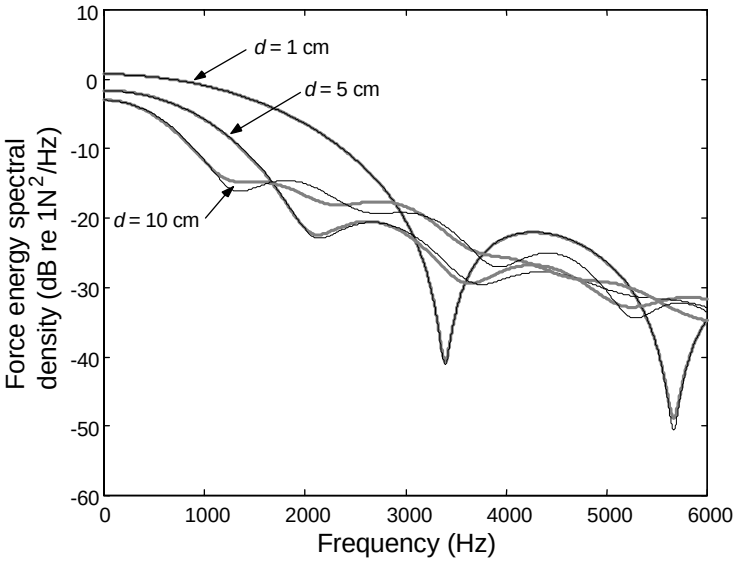

Fig. 8. Comparison of the force energy spectral densities of both forces for three different separation distances d, for a plate thickness $h = 3.18$ mm: ▬, force 1; ——, force 2.

4.4. Frequency response function calculation

Similarly to a force, the moment of a couple M_C typically generates translation as well as rotation of the structure. The mobility matrix as well as other types of FRFs shown in this section are calculated as follows:

1. the forces $F_1(t)$ and $F_2(t)$ are calculated in the time domain by substituting the solutions of system (7) presented in Section 4.2.1 into Eq. (6);
2. the Fourier transform is used to calculate the frequency spectra of the resulting forces;
3. the Fourier spectra are introduced as external excitation acting on the simply supported plate to calculate the two FRFs between each force location and the desired response point.

Using this approach, two FRFs were calculated, and the results are shown in Fig. 9 for the plate of thickness 3.18 mm used in the experimental validation at the end of the paper. Fig. 9a shows the ratio of the rotational velocity obtained from the action of the two forces $F_1(t)$ and $F_2(t)$, over the moment M_C generated by these two forces according to the relation

$$M_C = (F_1 + F_2)\frac{d}{2}. \tag{15}$$

Fig. 9b shows the ratio of the translational acceleration over the moment M_C. In each case, two curves are shown. The "moment with ideal forces" curve (thick line) assumes that both forces have rigorously equal magnitudes. The thin line curve uses the forces F_1 and F_2 calculated with the model developed in the previous sections. Although these forces take into account the coupling

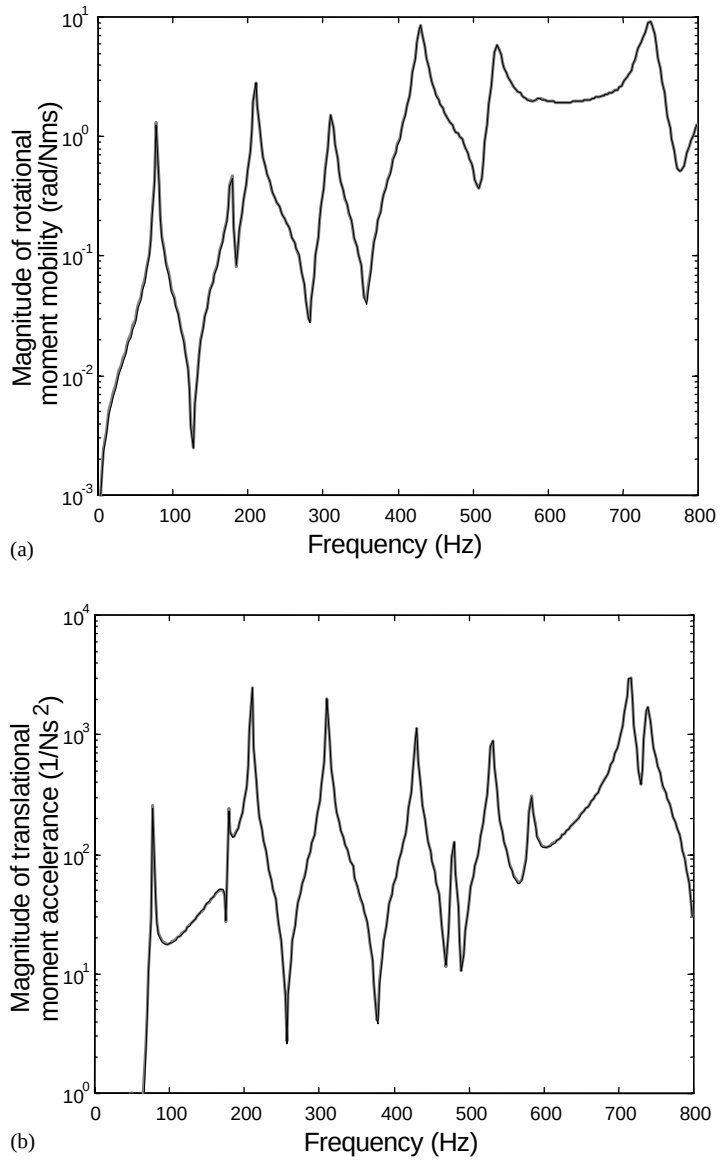

Fig. 9. Ratio of the rotational velocity (a) and translational acceleration (b), generated by two forces F_1 and F_2 separated by the distance d, over the moment $M_C = (F_2 + F_1)d/2$ generated by these forces. Plate thickness: $h = 3.18$ mm; force locations: F_1 (17 cm, 22.5 cm); F_2 (17 cm, 25.5 cm); response at (17 cm, 30 cm). ▬, moment with ideal identical forces; ——, moment with realistic calculated forces.

between the plate and the hammers, the two sets of results match almost perfectly and the difference between the curves is always smaller than a fraction of a dB.

It can then be concluded that, in this frequency range and for the considered plate, it is possible to obtain a set of two forces that can be considered as a couple, despite the coupling between the hammers and the plate.

5. Experimentation

5.1. Experimental device description

In order to experimentally implement the proposed technique, a device that can apply two controlled and synchronized impacts was fabricated. The block diagram of the system is shown in Fig. 10. The system uses two small brushless three-phase permanent magnets. The motors are controlled by a DSP board equipped with a TMS320F240 DSP, incorporating analog I/Os motor bridge and position sensors. Using mechanical adapters, a PCB miniature impulse force hammer model 086D80 was installed on the shaft of each motor. The force transducer signal is powered by a PCB ICP signal conditioner model 482A17. The force signals are filtered (low pass) by a Rockland Dual Hi/low filter model 852. The signals are then sent to the DSP card. The card is connected to a PC via a RS232 interface connection.

Both the magnitude and the synchronization of the two impact forces must be controlled. This is performed through an optimization procedure, using repeated hits. At each hit, the error in magnitude between the two forces is characterized by the difference of the time integral of the force signals. The time shift is evaluated by the time where the cross-correlation function of the force signals is maximum. The system calibrates itself by adjusting the signals provided respectively to each motors.

An aluminum plate with the same dimensions as the plate described in Section 4.2.2 is used. The plate is fixed to a heavy frame via a flexible thin connection plate in order to obtain simply supported boundary conditions. Fig. 11 shows two pictures of the system. Small plastic targets are glued to the plate at the impact points. They are used to control the frequency content of the force impulse (only one target on each side of the plate is of use, the second one gives an idea of the distance between the impact points). A relative calibration procedure was used to correct any relative sensitivity variation between the force transducers. Each hammer, driven by its own motor, was used to hit on a third force transducer fixed to a large rigid mass. Using the fixed force transducer measurement as the reference signal, a correction taking into account the specific behavior of each hammer was then applied to the sensitivity of each hammer.

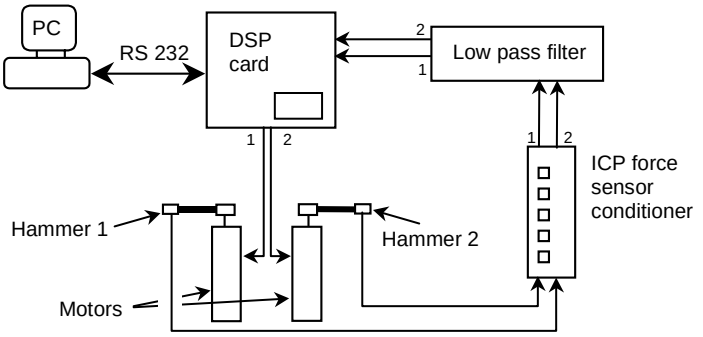

Fig. 10. Schematic description of the moment impacting device.

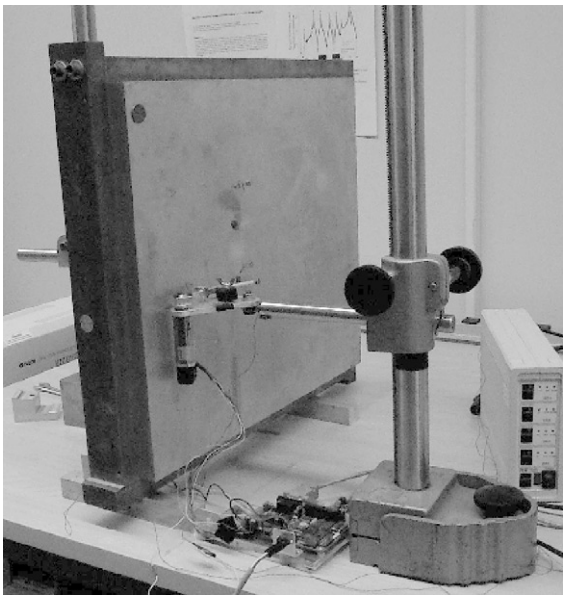

(a)

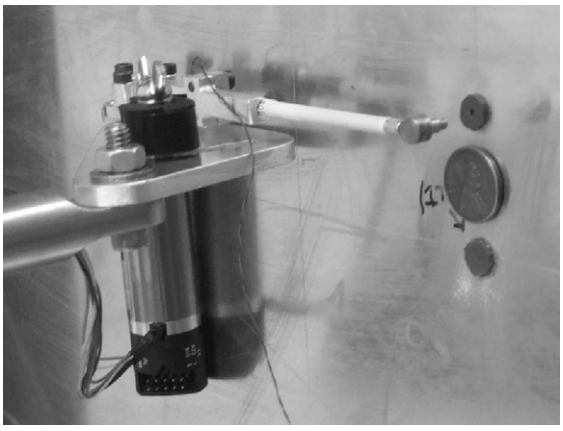

(b)

Fig. 11. Pictures of the plate and the impact system. (a) Only one hammer can be seen from these view angles, the second hammer being hidden by the plate. (b) On the closer view, impact plastic target can be seen. A coin is temporarily glued between the two targets to give a scale reference.

5.2. Result analysis

Fig. 12 shows the measured energy spectral density of the two forces. A force separation distance of 10 cm is used. The spectrum is not flat at the beginning of the frequency range as one would normally expect for an impact because of the filtering effect of the high pass filter of the analyzer. The two curves are very similar, which indicates that the system seems to control adequately the two impacts.

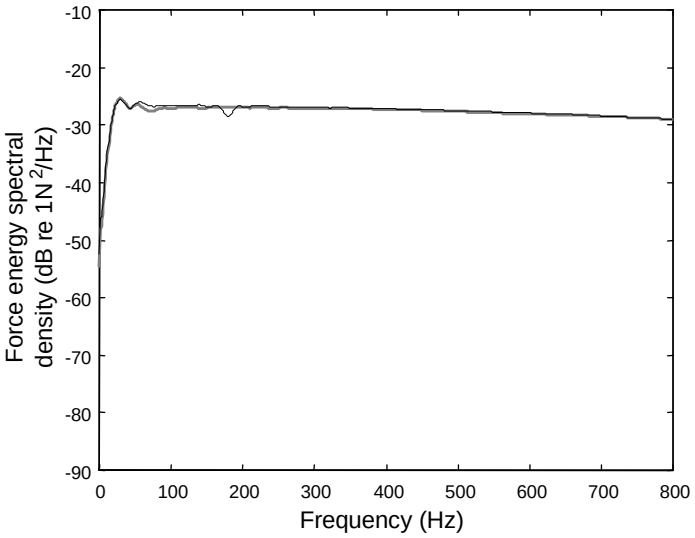

Fig. 12. Energy spectral density for the two impact forces. Distance between forces: $d = 10$ cm. Force 1 located at (17 cm, 19 cm); ——, force 2 located at (17 cm, 29 cm).

Another quality indicator is obtained by comparing the individual FRFs measured when both forces are active. If both forces are identical, the individual FRFs between the acceleration output and each force taken individually should be identical. Fig. 13 compares the magnitude and phase of the two FRFs. The curves overlay almost perfectly, which indicates that the two forces can be considered almost identical. It is interesting to note that it is always possible to measure these spectra. They can readily be used as a quality indicator to make sure that the impacting system provides a nearly pure couple.

Moment accelerance FRFs are compared for a force separation distance d of 3 cm in Fig. 14, and 10 cm in Fig. 15. Each figure shows in thin line the experimental frequency spectrum of the ratio between the accelerance measured at a point divided by the moment generated by the two impact forces applied elsewhere on the plate. The moment is calculated according to Eq. (15). The theoretical curves (thick lines) represent the FRF between a pure moment applied in the appropriate direction at the mid-point between the forces (17 cm, 24 cm) and the acceleration at the point (17 cm, 30 cm). Simply supported plate boundary conditions are assumed for the calculation and one single damping coefficient is used for all the modes. Note that the first peak at 20 Hz is associated with the rigid body mode of the support fixed to the table. The agreement between the theoretical and the experimental curves is excellent despite the difficulty of fabricating a simply supported plate that would offer nearly perfect theoretical boundary conditions.

For a force separation distance of 3 cm (Fig. 14), one can notice some discrepancies between the theoretical results and the measurement for the first two modes at 80 and 176 Hz. In addition, despite the averaging process, some noise remains on the measurements at lower frequencies. For a force separation distance of 10 cm (Fig. 15), the same two modes are measured correctly and noise effects are reduced. This is expected since a large separation distance will generate a moment with magnitude that will succeed to excite the lower modes associated with longer bending wavelength. Consequently, to be able to excite modes with large wavelength, a combination of large separation

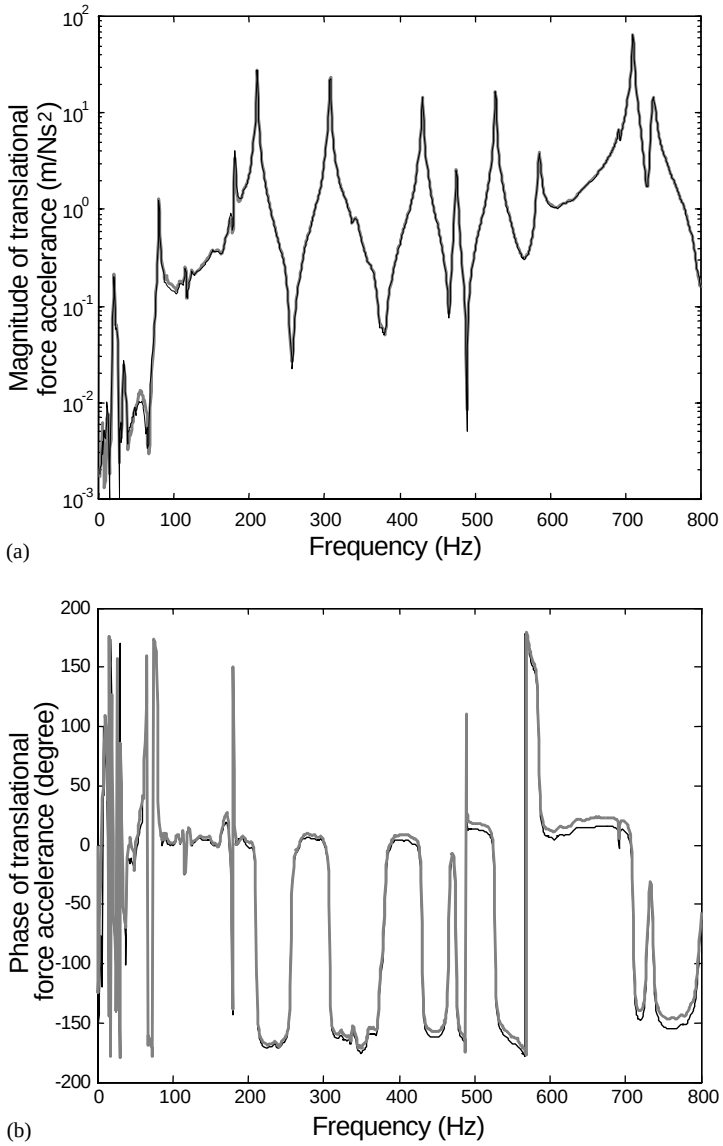

Fig. 13. (a) Magnitude and (b) phase of the FRFs measured simultaneously for both forces during the moment impact testing. Force locations: F_1 (17 cm, 19 cm); F_2 (17 cm, 29 cm); distance between forces: $d = 10$ cm; acceleration location at (17 cm, 30 cm). ▬, FRF using F_1 as the reference; ——, FRF using F_2 as the reference.

distance and high force magnitude should be used. To excite higher modes, a smaller separation distance should be used to avoid the bias created by the use of two forces. For a distance $d = 10$ cm with the plate used in this section, this bias effect appears only above 1000 Hz.

The appropriate selection of separation distances and force amplitudes will depend on the structure tested, and more specifically, on the modes wavelength. With this impacting technique requiring no attachment fixture, it is rather easy to change the configuration setup. Several

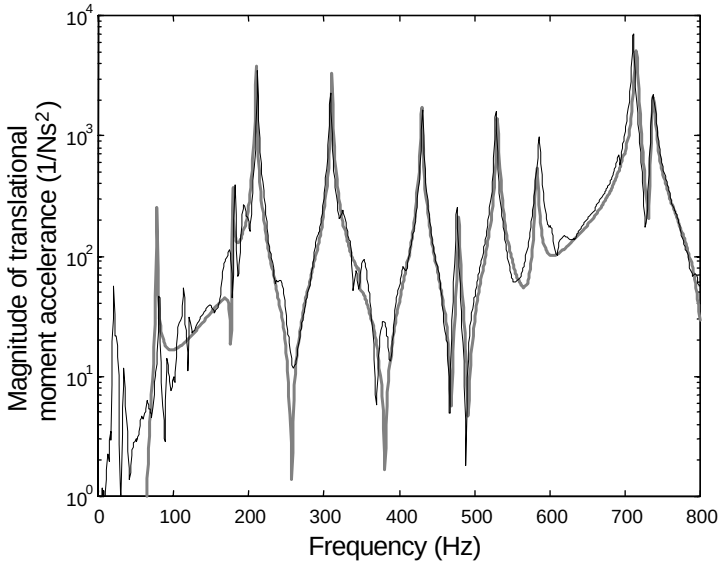

Fig. 14. Ratio between the translational acceleration and a moment. Force locations: F_1 (17 cm, 22.5 cm); F_2 (17 cm, 25.5 cm); distance between forces: $d = 3$ cm; Acceleration location (17 cm, 30 cm). ——, Theoretical result using a pure moment; ——, experimental result with a moment generated by the two impact measured forces F_1 and F_2.

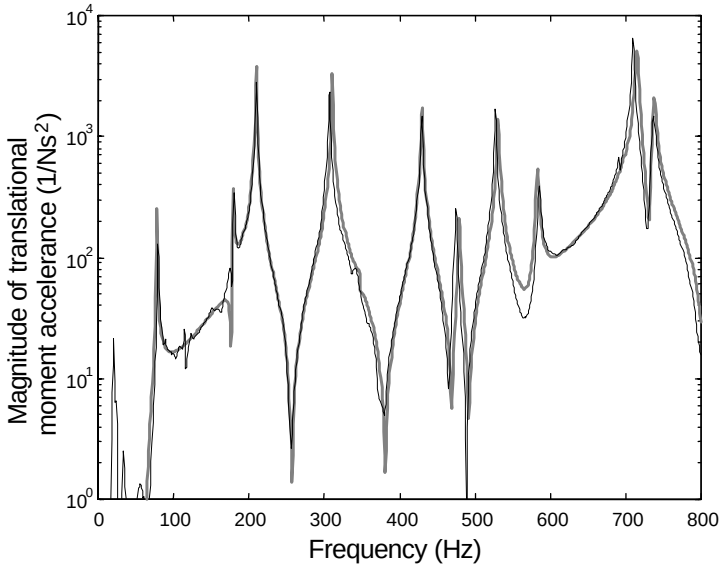

Fig. 15. Ratio between the translational acceleration and a moment. Force locations: F_1 (17 cm, 19 cm); F_2 (17 cm, 29 cm); distance between forces: $d = 10$ cm; acceleration location (17 cm, 30 cm). ——, theoretical result using a pure moment; ——, experimental result with a moment generated by the two impact measured forces F_1 and F_2.

separation distances can then be used in order to obtain accurate results. This is similar to the measurement of acoustic intensity where different microphone separation distances are used to measure intensity over the whole frequency spectrum.

6. Concluding remarks

The technique that uses two forces for generating moments has been employed for several years. In this paper, two impact hammers are used to generate the forces. Since the two forces are applied on each side of a plate, no additional fixtures are needed. It was first necessary to study how two distant identical forces can generate an almost pure moment. Then, a model that uses one degree of freedom to represent the behavior of an impact hammer and that takes into account the coupling between a simply supported plate and the hammers was developed. It has been shown that two synchronized hammers hitting the structure at the same initial velocity would generate forces that are very similar at all times. In the usable frequency range, the frequency spectra of the two forces do not differ by more than a fraction of a dB. Theoretical translational moment accelerance and rotational moment mobility have been calculated taking into account the coupling between the forces impact hammer and the structures. The results have been compared to the same quantities obtained with ideal identical forces. Despite the coupling, the two impact hammers succeed in generating forces that mimic a pure couple.

An experimental device to control the forces applied on each side of a plate by two impact hammers has been fabricated and tested. It was shown that, in the case of a thin homogeneous plate, the impact forces applied simultaneously are almost identical. The measured translational moment accelerance agrees very well with the theoretical results. Different force separation distances may be selected to test the whole frequency range of interest.

Acknowledgements

The authors would like to acknowledge D. Matchéto and B. Gauthier who contributed to this work respectively during their master's degree and engineer-training period at the Université de Sherbrooke.

References

[1] M.A. Sanderson, C.R. Fredö, Direct measurement of moment mobility, Part I: a theoretical study, Journal of Sound and Vibration 179 (4) (1995) 669–684.
[2] M.A. Sanderson, Direct measurement of moment mobility, Part II: an experimental study, Journal of Sound and Vibration 179 (4) (1995) 685–696.
[3] D.J. Ewins, P.T. Gleson, Experimental determination of multidirectional mobility data for beams, The Shock and Vibration Bulletin 45 (5) (1975) 153–173.
[4] J.E. Smith, Measurements of the total structural mobility matrix, The Shock and Vibration Bulletin 40 (7) (1969) 51–84.
[5] B. Petersson, On the use of giant magnetostrictive devices for moment excitation, Journal of Sound and Vibration 116 (1) (1987) 191–194.
[6] M.A. Stebbins, J.R. Blough, S.J. Shelley, D.L. Brown, Measuring and including the effects of moments and rotations for the accurate modeling of transmitted forces, Proceedings of the 14th IMAC, Dearbom, MI, 1996, pp. 429–436.
[7] T. Yoshimura, M. Hosoya, FRF estimation on rotational degrees of freedom of structures, Proceedings of the 18th IMAC, San Antonio, TX, 2000, pp. 1667–1671.

[8] S. Jianxin, B.M. Gibbs, Measurement of point moment mobility in the presence of non-zero cross mobility, Applied Acoustics 54 (1) (1998) 9–26.
[9] Y. Champoux, O. Beslin, B. Gautier, D. Machéto, B. Paillard, Moment mobility measurement using an impact force couple, Proceedings of the 25th ISMA, Leuven, Belgium, 2000, pp. 989–996.
[10] Y. Champoux, B. Paillard, D. Machéto, Moment excitation using two synchronized impact hammer, Proceedings of the 19th IMAC, Kissimmee, FL, 2001, pp. 543–549.
[11] C.D. Van Karsen, E.F. Little, The strengths of impact testing, Proceedings of the 15th IMAC, Orlando, FL, 1997, pp. 1667–1671.
[12] D. Brown, Weaknesses of impact testing, Proceedings of the 15th IMAC, Orlando, FL, 1997, pp. 1672–1676.
[13] L. Ivarsson, M.A. Sanderson, A.G. Troshin, Design, theory and validation of a low mass 6-d.o.f. transducer, Journal of Sound and Vibration 230 (3) (2000) 661–688.